A Poor Relationship Between Sea Level and Deep-Water Sand Delivery Keywords Sea-level Change Stratigraphic Forward Modelling Sequence Stratigraphy Accommodation DeepWater Sediment Transport

Ashley D Harris, Sarah E Baumgardner, Tao Sun, Didier Granjeon

A Poor Relationship Between Sea Level and Deep-Water Sand Delivery

Authors

Ashley D. Harris (a), Sarah E. Baumgardner (a), Tao Sun (a), Didier Granjeon (b)

Affiliation

(a) Chevron Energy Technology Company, Houston, Texas 77002, USA

(b) IFP Energies Nouvelles, 1 à 4 avenue de Bois, Préau, 92852 Rueil-Malmaison, France

Keywords

Sea-level Change

Stratigraphic Forward Modelling

Sequence Stratigraphy

Accommodation

DeepWater

Sediment Transport

Abstract

The most commonly cited control on delivery of sand to deep water is the rate of relative sea-level fall. The rapid rate of accommodation loss on the shelf causes sedimentation to shift basinward. Field and experimental numerical modeling studies have shown that deep-water sand delivery can occur during any stage of relative sea level position and across a large range of values of rate of relative sea-level change. However, these studies did not investigate the impact of sediment transport efficiency on the relationship between rate of relative sea-level change and deep-water sand delivery rate. We explore this relationship using a deterministic nonlinear diffusion-based numerical stratigraphic forward model. We vary across three orders of magnitude the diffusion coefficient value for marine settings, which controls sediment transport efficiency. We find that the rate of relative sea-level change can explain no more than 1% of the variability in deep-water sand delivery rates, regardless of sediment transport efficiency. Model results show a better correlation with relative sea level, with up to 55% of the variability in deepwater sand delivery rates explained. The results presented here are consistent with studies of natural settings which suggest stochastic processes such as avulsion and slope failure, and interactions among such processes, may explain the remaining variance. Relative sea level is a better predictor of deep-water sand delivery than rate of relative sea-level change because it is the sea-level fall itself which promotes sand delivery, not the rate of the fall. We conclude that the poor relationship between sea level and sand delivery is not an artifact of the modeling parameters but is instead due to the inadequacy of relative sea level and the rate of relative sea-level change to fully describe the dimensional space in which depositional systems reside. Subsequently, sea level itself is unable to account for the interaction of multiple processes that contribute to sand delivery to deep water.

1. Introduction

Understanding the causal mechanism for sediment distribution on continental margins is crucial to the identification of economic hydrocarbon reservoirs, prediction of geohazards, and selection of sites for carbon sequestration (Vail et al., 1977; Urlaub et al., 2013; Miller et al., 2017). The hypothesis that marine sediment distribution is due to accommodation change as the result of variation of relative sea level (i.e., the combined effects of eustasy, tectonism, crustal cooling, sediment compaction, and loading) has been the dominant sequence stratigraphic conceptual model since the 1980's (Jervey, 1988; Posamentier et al., 1988; Posamentier and Allen, 1999). Specifically, interpretations using this model have focused on the rate of relative sea-level change, which is the first derivative of the eustatic curve minus the first derivative of subsidence, because the rate of relative sea-level change controls the rate of reduction or addition of space available for potential deposition (i.e., accommodation; Jervey, 1988). This classic model has been used to suggest that the coarsest-grained material is deposited in deeper water during the time period from the maximum rate of relative sea-level fall, when the rate of loss of accommodation is the greatest on the shelf, to the subsequent (local) minimum value of relative sea level (Posamentier and Kolla, 2003; Catuneanu et al., 2009) (Fig. 1). According to this paradigm, peaks in deep-water sand delivery rates will therefore coincide with the most negative to zero values of rate of relative sea-level change (Catuneanu et al., 2009). However, field studies have shown that sediment transport dynamics and a basin's climatic and tectonic setting may overwhelm the effect of the relative sea-level change on the rate of delivery of sediment to deep water (Carvajal et al., 2009; Covault and Graham, 2010; and references therein; Dixon et al., 2012; Toucanne et al., 2012; Bourget et al., 2014; Talling, 2014; Liu et al., 2016; Allin et al., 2018). In these examples, oceanographic processes, seismic activity, narrow shelves, or high sediment supply contribute to the delivery of sand beyond the shelf edge during the rise or highstand in sea level.

Recent numerical stratigraphic forward modeling experiments have also shown that the relationship between deep-water sand delivery rate and relative sea level is weak (Harris et al., 2016). In these experiments, a series of eustatic curves were applied to a passive margin to study the effects of relative sea level on the total volume of sand delivered to deep water as well as on the timing and magnitude of delivery events. Model results showed that peaks in deep-water sand delivery occurred during both the falling and rising limbs of relative sea level and that the magnitude of deep-water sand delivery did not correspond to the magnitude of the sea-level fall. The models further demonstrated that autogenic processes (i.e., shelf-edge delta avulsion) could produce fluctuations in deep-water sand delivery rate with magnitudes similar to those driven by sea-level falls as well as comparable total volumes. The implications of these experiments are that autogenic processes, small, and large sea-level falls can each produce similar depositional system responses and that the timing of such responses may not be predictable from the eustatic record. Harris et al. (2016) attributed the invariant response of the sedimentary system to the concept of self-regulated equilibrium regression of shelf-edge deltas (sensu Burgess et al., 2008). This state occurs when the initial progradation of a delta to the shelf edge creates a slope that is conducive to the efficient transport of sediment across the shelf, which in turn allows subsequent progradational events to deposit sediment in deep water regardless of the magnitude of sediment supply or sea-level changes. These insights on the response of a sedimentary system to autogenic processes and sea-level changes were derived from diffusion-based numerical stratigraphic forward models (SFMs) (Burgess et al., 2006, 2008; Harris et al., 2016). Diffusion-based SFMs simulate water and sediment movement

across a digital elevation model (see Fig. 2 of Prince and Burgess, 2013). The main assumption of diffusion models is that they can effectively capture the first-order evolution of sedimentary systems at spatial scales of meters to kilometers and temporal resolution of thousands of years (Granjeon, 2014). Such models have been validated through comparison of numerically-produced results to the large-scale stratal architecture and facies distributions observed in numerous sedimentary basin settings (Flemings and Jordan, 1989; Jordan and Flemings, 1991; Clevis et al., 2003; Csato et al., 2013, 2015; Granjeon, 2014). The most challenging task in using diffusion-based sediment transport models is identification of the appropriate values for the diffusion coefficients. These values control the efficiency of sediment transport within the model and therefore can have as significant impact on sediment distribution as sea level, sediment and water supply (Rivenæs, 1997; Burgess et al., 2006, 2008; Gvirtzman et al., 2014). Previous studies have applied values which span several orders of magnitude; modelers often adjust the diffusion coefficients until the model produces slopes or stratal geometries analogous to those of the settings of interest.

Higher water-driven marine diffusion coefficients can cause fluvial-deltaic discharge to behave more like a plunging or hyperpycnal flow, bypassing sand to deeper parts of the basin with minimal influence from sea level, rather than an expanding or buoyant flow which deposits sand at the terminus of a fluvial system (Rivenæs, 1997; Gvirtzman et al., 2014). Therefore, higher water-driven diffusion coefficients for sand in marine settings should yield increasingly poor correlations between fluctuations in sea level and deep-water sand delivery, and lower values should improve the relationship, but the extent of this potential effect has not been tested systematically by previous workers. Here, we develop a series of numerical models to test the classic sequence stratigraphic conceptual model by exploring the effects of sediment transport efficiency on the relationship between deep-water sand delivery rate and sea level. We analyze this relationship by extracting deep-water sand delivery time series from each model and conducting regression analysis of both relative sea level and the rate of relative sea-level change versus that of deep-water sand delivery. Numerical modeling experiments provide an opportunity to refine sequence stratigraphic concepts through quantitative assessment of the role of relative sea-level change in continental margin sand distribution and examining the assumptions of diffusion-based numerical stratigraphic models.

2. Methods

2.1. Assumptions and Mechanics of Dionisos

Dionisos is a deterministic three-dimensional numerical stratigraphic forward model developed to simulate sediment transport at the basin scale (Granjeon, 2014). The model is used to examine the interaction of tectonism, sea level, water, and sediment supply as they relate to the volume and architecture of sedimentary deposits in the basin. Sediment transport in Dionisos is governed by overland water flow routing and a nonlinear sediment transport law (Granjeon, 2014). Overland flow is water that flows horizontally across a surface when the precipitation rate exceeds the capacity to infiltrate the surface (Horton, 1933). Overland flow water routing utilizes a multiple flow direction algorithm which can allow water to be proportionally distributed to adjacent downstream cells according to local slope. The nonlinear sediment transport law is comprised of two main equations: nonlinear hillslope creeping (gravity-), and fluvially- (water-) driven processes. This is a method of parametrizing sediment transport comparable to that used by other well-known stratigraphic forward models and validated by field studies (e.g., Willgoose et al., 1991; Rivenæs, 1992, 1997;

Tucker and Slingerland, 1994; Flemings and Grotzinger, 1996; Paola, 2000). The combined equation is:

$$Q_S = -\left(K_s + K_w q_w^n \left\|\vec{\nabla} h\right\|^{m-1}\right)\vec{\nabla} h$$

where Qs is sediment flux (km2/kyr); Ks and Kw are the hillslope and water-driven diffusion coefficients, respectively (km2/kyr); qw is the dimensionless water flux (-) which is the water discharge input value (m3/s) normalized by the reference discharge value of 1 m3/s; h is the topographic elevation (m); and ∇h is the local topographic gradient or slope (-) (Granjeon, 2014).

The model solves this equation for sand and mud grain size classes in the experiments detailed here. Sediment transport efficiency of each grain size class is governed by different diffusion coefficients for subaerial ("terrestrial") and subaqueous ("marine") settings. Therefore, each grain size class has two hillslope and two water transport diffusion coefficients: a total of eight coefficients for each model. In accordance with other diffusion-based basin- fill models, subaqueous or marine diffusion coefficient values are lower than subaerial values to reflect reduced sediment transport rates and increased deposition as fluvial systems enter water-filled basins (Kaufman et al., 1991; Rivenæs, 1992, 1997; Flemings and Grotzinger, 1996). This experiment examines the strength of the relationship between the sea-level change and deep-water sand delivery by analyzing seven models that vary over several orders of magnitude the values of the water-driven marine diffusion coefficient for sand (Kw, marine, sand) (Table 1). Gvirtzman et al. (2014) demonstrated that higher diffusion coefficients increase sediment transport efficiency and simulate a plunging or hyperpycnal flow at the mouth of the river and lead to the development of submarine fans on the basin floor. Dionisos assumes a quasi-steady state continuous turbidity flow and therefore simulates the aggregate long-term evolution of turbidity systems as opposed to individual turbidity flows or turbulence itself. Sediment is also transported downdip through slope failure processes, triggered for all sediment classes by slopes exceeding 2° (Table 2).

The nonlinear sediment transport law implemented in Dionisos allows it to simulate autogenic processes such as avulsion through the adjustment of sediment transport capacity related to slope and water- driven transport (n and m exponents, respectively). Increased water flow can localize erosion, creating incision or channelization due to increased sediment transport capacity; decreased water flow results in deposition due to reduced transport capacity. These processes combine to cause large-scale avulsion: deposition at the distal end of the sedimentary systems related to low slope or water-flow conditions causes backfilling, elevation of the fluvial plain or submarine canyon floor, and water flow migration. Avulsion is therefore entirely controlled by the routing of water and sediment across the modeled area, rather than by any set of boundary conditions imposed by the user.

2.2. Model Setup

2.2.1. Initial Bathymetry and Tectonics

The model dimensions were 800 km (x-direction) by 800 km (y-direction) with 10 km grid point spacing (Fig. 2). A domain of this size permitted sedimentary processes to occur with minimal boundary effects while allowing the model to be computationally efficient. The initial bathymetry was a ramp setting with a slope of 0.06° with the first 100 km of the proximal portion subaerially exposed, which increased to a water depth of 695 m at the distal edge of the basin. The slope of the initial bathymetry is similar to that of typical passive margin shelves (Table 2).

We elected to use a ramp setting rather than a pre-formed margin to allow the sedimentary system in each model to develop its own major physiographic features. Deep-water sand delivery is defined as sand deposited in water at or below the 200 m isobath as defined for that time step. This depth is the deepest part of the neritic zone and often corresponds to the shelf edge. The model implemented a simple, hinge-style tectonic subsidence with a rate of 0 m/Myr in the most proximal position and which linearly increased to 100 m/Myr at the most distal position.

2.2.2. Sea level

Each model used the eustatic curve of Kominz et al. (2008), which contributed to changing accommodation through time. The model ran with 0.1 Myr timesteps spanning the period from 66 Ma to 10 Ma. This period was characterized by a long-term cooling in average global temperatures and corresponding fall in sea level (Miller et al., 2005, 2011). The eustatic curve over this interval consisted of 20-60 m 3rd order sea- level changes (Miller et al., 2005, 2011; Kominz et al., 2008; Harris et al., 2010). This study did not include the N 60 m sea-level changes of the last 3 Myr, though the differences in the dynamics of sedimentary systems in icehouse and greenhouse settings continues to be an ongoing topic of investigation (Sømme et al., 2009; Li et al., 2016). Relative sea level and the rate of relative sea-level change were calculated from a position 200 km downdip of the most proximal edge of the model, 100 km downdip of the initial shoreline. The rate of relative sea-level change was calculated by subtracting the rate of subsidence (25 m/Myr) at this position from the rate of eustatic change.

2.2.3. Sediment Supply

Constant sediment and water discharge rates analogous to medium-sized fluvial systems were applied to the models to be consistent with sequence stratigraphic models (sensu Posamentier et al., 1988) (Fig. 3). A medium-sized fluvial system ensured sedimentation across the modeled domain and allowed the development of a shelf margin or submarine canyon system over the modeled period. All model cases included a sediment load and initial substrate composed of 20% sand and 80% mud. These values are similar to those used in other numerical modeling studies (e.g., Burgess et al., 2006) and are in accord with notion that the majority of the sedimentary rock record consists of fine-grained material (Picard, 1971; Schieber and Zimmerle, 1998). Both the initial surface and the sediment deposited during the model run had a maximum mechanical erosion rate of 1000 m/Myr. The actual erosion rate was determined by the sediment transport assumptions described above; no model run in this study reached the prescribed maximum erosion rate.

3. Results

3.1. Deep-water Sand Delivery and Stratal Architecture

The Kw, marine, sand (water-driven subaqueous sand diffusion coefficient) value had a major impact on the stratal architecture and sand distribution (Fig. 4). Sedimentary systems formed with lower diffusion coefficient values (Model Runs 1-5; see Table 1) produced continental shelves, whereas those with higher values (Model Runs 6-7; see Table 1) incised the initial bathymetry and delivered increased volumes of sand to deep water. In models 1-5, sand was delivered to deep-water through slope failure at the shelf edge and the influence of sea-level fluctuations is well represented in their respective deep-water sand delivery rates: the timing of peak values of sediment delivery corresponds to periods of falling sea level. However, the magnitude of deep-water sand delivery

does not correspond with the magnitude of sea-level change (Fig. 5). In model 1, a 25 m sea-level fall at 15.2 Ma produced a peak in deep-water sand delivery rate larger than the 65 m fall at 40 Ma. Other examples of the invariant response of the sedimentary system may be found in the interval between 18-15.5 Ma, where two sea-level falls of 26 m and 21 m produced peaks in deep-water sand delivery similar to one occurring in the eustatically-stable highstand interval between them. Yet, a minor fall during the subsequent highstand resulted in a significant peak in deep-water sand delivery.

In the higher diffusion coefficients of models 6 and 7, sand was bypassed to deep water through the development of a canyon (Fig. 4). The fluctuations in deep-water sand delivery were due to repeated avulsions of the channel on the basin floor fan and flushing of the canyon (Fig. 5). Sediment accumulated on the basin-floor fan and at the base of the canyon which caused backfilling, elevation of the canyon floor, and subsequent flushing events. Fluctuations in deep-water sand delivery rate were also caused by slope failure on the canyon walls. These processes often resulted in multiple peaks in deep-water sand delivery rates for a single sea-level fall. For example, in model 7, five peaks in deep-water sand delivery correspond to a single 65 m sea-level fall starting at 40 Ma (Fig. 5).

Differences in the nature of deep-water sand delivery are also illustrated in the normalized cumulative deep-water sand volume curves (Fig. 6). The stepped behavior of the curves for models 1-5 show intervals of rapid, large-voluminous deep-water sand delivery for lower Kw, marine, sand values. The higher Kw, marine, sand values of models 6 and 7 resulted in a more constant delivery of deep-water sand and thus a smoother, more linear, curve, explaining the higher minimum values of deep-water sand delivery rates than those in models 1-5 (Figs. 3, 4).

Increasing the Kw, marine, sand values had an impact on the frequency distribution of the deep-water sand delivery rates (Fig. 7). Models 1-4 have distributions that approach log-normal, with the largest frequency of deep-water sand delivery rates corresponding to lower values and lower frequency of events for higher values. Model 5 has a distribution that is distinct from the other models in that the frequency of deepwater sand delivery rates approaches a more uniform distribution, though it appears to be multimodal. Models 6 and 7 have deep-water sand delivery rate distributions that approach normal with higher mean values and a decrease in lower values with respect to Models 1-4.

3.2. Regression Analysis of Deep-Water Sand Delivery and Sea Level

Linear regression analysis was conducted on the relationship between deep-water sand delivery, relative sea level and rate of relative sea-level change. Relative sea level explains 55% of the variance in deepwater sand delivery in the best-case scenario (Model 5; Table 3). Overall, there is a positive correlation between the Kw, marine, sand value and variance explained up to Model 5. Models 6 and 7 show a progressive decrease in variance explained.

No model cases show a strong relationship between deep-water sand delivery rate and rate of relative sea-level change (Fig. 8). Increasing Kw, marine, sand values produced an inverse relationship with r2 values as hypothesized. Overall, no model in the entire experimental design achieved an r2 value greater than 0.01, thus suggesting that the rate of relative sea-level change alone is not a dominant control on deepwater sand delivery.

4. Discussion

According to classic sequence stratigraphic conceptual models, an increase in the sand/mud ratio or grain size delivered to deep water will correspond to the fastest rate of sea-level fall to the sea-level minimum (where the rate of change is zero; Posamentier et al., 1988; Posamentier and Allen, 1999;

Catuneanu et al., 2009). Recent numerical modeling experiments have demonstrated that there is a poor relationship between deep-water sand delivery and sea level, assuming all other parameters constant (Harris et al., 2016). These experiments used a diffusion-based numerical stratigraphic forward model to examine the impact of different eustatic curves on continental margin sand distribution and could identify no distinguishing characteristics in spatial pattern. In the experiments presented here, we examined the influence of the sediment transport efficiency on the relationship between deep-water sand delivery and sea level. The diffusion coefficient controls sediment transport efficiency and has been demonstrated to significantly impact sediment distribution and stratal architecture (Rivenæs, 1997; Gvirtzman et al., 2014).

Our model results show that there is generally a poor relationship between deep-water sand delivery rate and sea level in all model scenarios, though sediment transport efficiency did impact shelf-margin architecture (Fig. 4). The r2 values in the best-case scenarios for relative sea level and rate of relative sea-level change can explain no more than 55% and 1% of the variability in deep-water sand delivery rates, respectively. The variance in deep-water sand delivery rate explained by relative sea level positively correlated with an increase in Kw, marine, sand values, which is counter to this study's initial hypothesis. That is because increasing the efficiency of sediment transport improved the fluvial-deltaic systems' response to sea-level fluctuations up to a certain value (Model 5). Beyond this value, the sediment transport became so efficient that the sedimentary system decreasingly relied on sea level to deliver sand to deep water. This conclusion is supported by the shelf margin architecture, where increasing sediment transport efficiency values produced a less pronounced shelf (Models 1-5) and a submarine canyon system in the highest values (Models 6-7). The connection between the sediment and water point source becomes more direct with the higher Kw, marine, sand values due to lack of a shelf or staging zone (sensu Posamentier and Kolla, 2003) and thus produces a smoother, more linear deep-water sand delivery curve (Fig. 6). Relative sea level can explain more of the variance in deep-water sand delivery than rate of relative sea-level change because it is the presence of a sea-level fall itself rather than the rate of that fall which delivers sand to deep water. This is very well illustrated in study of Harris et al. (2016) where peaks in deep-water sand delivery rates correspond to lowstand intervals, yet those peaks occurred during the local minimum, rise and fall of sea level.

The frequency distribution of deep-water sand delivery rate changed with the imposed value of sediment transport efficiency. Models 1-4 show distributions that approach log-normal. Log-normal distributions are a common occurrence in geology and observed in deep-water settings with respect to turbidite bed thickness and recurrence intervals (Davis, 1986; Sylvester, 2007; Pantopoulos et al., 2013; Clare et al., 2016; Allin et al., 2018). The product of the occurrences of two or more normally-distributed random variables results in a log-normal distribution (Davis, 1986). Studies that have observed log-normal distributions in turbidite occurrence on continental margins suggest the distribution is the result of the combination of different turbidite triggering mechanisms (e.g., earthquakes and littoral cells delivering sediment to the heads of canyons) rather than solely the product of sea level (Allin et al., 2018). In this study, sea level, avulsion, and slope failure all contribute to deep-water sand delivery. The interaction of these independent processes produces a behavior that is not wholly predictable from model inputs.

Model 5 shows a multimodal distribution that is not found in the other models. This model scenario also shows the strongest correlation between relative sea level and deep-water sand delivery. The multimodality of the distribution and relatively stronger correlation likely reflects the different size sea-level changes in the sea-level curve (Fig. 7). However, since only 55% of the variance in deep-

water sand delivery is explained by relative sea level, nearly half of the variance in the best-case scenario must be explained by other mechanisms, such as those discussed above. Model 5 is a transition from deep-water sand delivery rates that approach a log-normal distribution in models 1- 4 to those that approach a normal distribution in models 6 and 7. Larger deep-water sand delivery rates become more frequent and smaller values become rarer in models 6 and 7 (Fig. 7). In these models, the distribution is interpreted to reflect a more direct connection between the sediment and water point source and deep-water sand delivery. Nevertheless, in these models, avulsion, slope failure, and sea level interact to produce unsteady deep-water sand delivery.

The results of this modeling study and others (e.g., Kim et al., 2009; Harris et al., 2016) suggest that the poor relationship between sea level and deep-water sand delivery is independent of model input parameters and broadly consistent with field observations (e.g., Allin et al., 2016, 2018) and therefore representative of natural systems (Paola et al., 2009). This study and others have identified multiple controls on deep-water sand delivery and speculated that the interactions among these controls contribute to a poor relationship between sea level and deep-water sediment delivery. However, we posit that this lack of predictability also stems from a mismatch between the dimensions of relative sea level, rate of relative sea-level change (one-dimensional), and depositional system processes (four-dimensional). Rate of relative sea-level change is the rate of eustatic change minus the tectonic subsidence rate, which is taken at a point and can only practically be described as a one-dimensional time series (e.g., Figs. 10 and 13 of Posamentier et al., 1988). This time series is then used to describe the four-dimensional (x, y, z and time) character of sedimentary systems, creating a mismatch in dimensional space and implicitly excluding spatial variability, all but guaranteeing a poor correlation. Moreover, this emphasizes the poor dimensional descriptions of sedimentary systems in sequence stratigraphic concepts also highlighted by other workers (Muto and Steel, 2000; Burgess, 2016; Madof et al., 2016; Burgess, 2016; Zhang et al., 2017). Given this, we therefore recommend a broad-based approach to interpretation of the spatiotemporal distribution of deep-water sand deposits that incorporates depositional system context (e.g., climate, tectonism, sedimentary system dynamics, and marine processes) in multidimensional space, rather than solely focusing on sea-level change.

5. Conclusions

Sediment transport efficiency has been shown to have a significant influence on the response of a numerically-modeled sedimentary system to its boundary conditions and its resulting stratal architecture. We examined the long-term impact of the value of the water-driven marine diffusion coefficient for sand on the relationship between deep-water sand delivery and sea level. Model results show that there is a poor direct relationship between relative sea level, rate of relative sea-level change and sand delivery regardless of the choice of diffusion coefficient. We conclude that the use of sea-level change alone to describe changes in shelfal accommodation, and therefore deep-water sand delivery, is greatly hampered by the lack of dimensional space characterization and ignores the multiple combinations of processes that could contribute to deep-water sand sedimentation. The results presented here demonstrate that numerical SFMs are capable of producing outcomes that are similar to those observed in natural settings because they can account for multiple controls on sedimentation in multidimensional space. We therefore strongly recommend that the insights from well validated numerical models be given serious consideration in the continued development of sequence stratigraphic concepts.

Acknowledgement

The authors thank Chevron Corporation, Energy Technology Company for allowing us to publish this study. We thank Jimmy Bent, Andrew Madof, Tony Gary, and Mariana Harris-Ortega for very helpful discussions and support. We thank an anonymous reviewer and Michael Clare for insightful reviews that greatly improved the quality of the manuscript. We also thank the editor, Jasper Knight, for comments that clarified the main points of the paper. We also greatly appreciate a discussion with Jai Syvitski that sparked the idea for this study. Dionisos (now DionisosFlow) is currently being developed as a part of an industry consortium through IFP Energies Nouvelles. DionisosFlow is a commercially available software package from BeicipFranlab available at http:// www.beicip.com/stratigraphic-modeling-0.

References

Allin, J.R., Hunt, J.E., Talling, P.J., Clare, M.A., Pope, E., Masson, D.G., 2016. Different frequencies and triggers of canyon filling and flushing events in Nazaré Canyon, offshore Portugal. Marine Geology 371, 89–105.

Allin, J.R., Hunt, J.E., Clare, M.A., Talling, P.J., 2018. Eustatic sea-level controls on the flushing of a shelf-incising submarine canyon. GSA Bulletin 130, 222–237.

Booth, J.S., O'Leary, D.W., Popenoe, P., Danforth, W.W., 1993. U.S. Atlantic continental slope landslides: their distribution, general attributes, and implications. U.S. Geological Survey Bulletin 2002, 14–22.

Bourget, J., Ainsworth, R.B., Thompson, S., 2014. Seismic stratigraphy of a tide and wave dominated shelf-edge delta (NW Australia): process based classification from 3D seismic attributes and implications for the prediction of deep-water sands. Marine and Petroleum Geology 57, 359–384.

Burgess, P.M., 2016. Research Focus: The future of the sequence stratigraphy paradigm: Dealing with a variable third dimension. Geology 44, 335–336.

Burgess, P.M., Lammers, H., van Oosterhout, C., Granjeon, D., 2006. Multivariate sequence stratigraphy: Tackling complexity and uncertainty with stratigraphic forward modeling, multiple scenarios, and conditional frequency maps. AAPG Bulletin 90, 1883–1901.

Burgess, P.M., Steel, R., Granjeon, D., 2008. Stratigraphic forward modeling of basin margin clinoform systems: implications for controls on topset and shelf width and timing of formation of shelf-edge deltas. In: Hampson, G., Steel, R., Burgess, P.M., Dalrymple, R.W. (Eds.), Recent advances in models of siliciclastic shallow-marine stratigraphy. Society of Economic Paleontologist and Mineralogist, Special Publication 90, pp. 35–45.

Carvajal, C., Steel, R., Petter, A., 2009. Sediment supply: the main driver of shelf-margin growth. Earth-Science Reviews 96, 221–248.

Catuneanu, O., Abreu, V., Bhattacharya, J.P., Blum, M.D., Dalrymple, R.W., Eriksson, P.G., Fielding, C.R., Fischer, W.L., Galloway, W.E., Gibling, M.R., Giles, K.A., Holbrook, J.M., Jordan, R., Kendall, C.G.St.C., Macurda, B., Martinsen, O.J., Miall, A.D., Neal, J.E., Nummedal, D., Pomar, L., Posamentier, H.W., Pratt, B.R., Sarg, J.F., Shanley, K.W., Steel, R.J., Strasser, A., Tucker, M.E., Winker, C., 2009. Towards the standardization of sequence stratigraphy. Earth-Science Reviews 92, 1–33.

Clare, M.A., Talling, P.J., Challenor, P.G., Hunt, J.E., 2016. Tempo and Triggering of Large Submarine Landslides: Statistical Analysis for Hazard Assessment. In: Krastel, S., Behrmann, J.-H., Völker, D., Stipp, M., Berndt, C., Urgeles, R., Chaytor, J., Huhn, K., Strasser, M., Harbitz, C.B. (Eds.), Submarine Mass Movements and their Consequences. Springer International Publishing, pp. 509–517.

Clevis, Q., de Boer, P., Wachter, M., 2003. Numerical modelling of drainage basin evolution and three-dimensional alluvial fan stratigraphy. Sedimentary Geology 163, 85–110.

Covault, J.A., Graham, S.A., 2010. Submarine fans at all sea-level stands; tectonomorphologic and climatic controls on terrigenous sediment delivery to the deep sea. Geology 38, 939–942.
Csato, I., Granjeon, D., Catuneanu, O., Baum, G.R., 2013. A three-dimensional stratigraphic model for the Messinian crisis in the Pannonian Basin, eastern Hungary. Basin Research 25, 121–148.
Csato, I., Tóth, S., Catuneanu, O., Granjeon, D., 2015. A sequence stratigraphic model for the Upper Miocene–Pliocene basin fill of the Pannonian Basin, eastern Hungary. Marine and Petroleum Geology 66, 117–134.
Davis, J.C., 1986. Statistical Data Analysis in Geology. second ed. John Wiley & Sons, New York (646 pp.).
Dixon, J.F., Steel, R., Olariu, C., 2012. Shelf-edge delta regime as a predictor of deepwater deposition. Journal of Sedimentary Research 82, 681–687.
Flemings, P.B., Grotzinger, J.P., 1996. STRATA: Freeware for analyzing classic stratigraphic problems. GSA Today 6, 1–7.
Flemings, P.B., Jordan, T.E., 1989. A synthetic stratigraphic model of foreland basin development. Journal of Geophysical Research 94, 3851–3866.
Granjeon, D., 2014. 3D forward modelling of the impact of sediment transport and base level cycles on continental margins and incised valleys. In: Martinius, A.W., Ravnås, R., Howell, J.A., Steel, R.J., Wonham, J.P. (Eds.), Depositional Systems to Sedimentary Successions on the Norwegian Continental Margin. International Association of Sedimentologists, Special Publication 46, pp. 453–472.
Gvirtzman, Z., Csato, I., Granjeon, D., 2014. Constraining sediment transport to deep marine basins through submarine channels: The Levant margin in the Late Cenozoic. Marine Geology 347, 12–26.
Harris, A.D., Miller, K.G., Browning, J.V., Sugarman, P.J., Olsson, R.K., Cramer, B.S., Wright, J.D., 2010. Integrated stratigraphic studies of Paleocene — lowermost Eocene sequences, New Jersey Coastal Plain: evidence for glacioeustatic control. Paleoceanography 25, PA3211. https://doi.org/10.1029/2009PA001800.
Harris, P.T., McMillan-Lawler, M., Rupp, J., Baker, E.K., 2014. Geomorphology of the oceans. Marine Geology 352, 4–24.
Harris, A.D., Covault, J.A., Madof, A.S., Sun, T., Sylvester, Z., Granjeon, D., 2016. Three- dimensional numerical modeling of eustatic control on continental-margin sand distribution. Journal of Sedimentary Research 86, 1434–1443.
Horton, R.E., 1933. The role of infiltration in the hydrological cycle. Eos, Transactions American Geophysical Union 14, 446–460.
Jervey, M.T., 1988. Quantitative geological modeling of siliciclastic rock sequence and their seismic expression. In: Wilgus, C.K., Hastings, B.S., Kendall, C.G.S., Posamentier, H.W., Ross, C.A., Van Wagoner, J.C. (Eds.), Sea-level Changes: An Integrated Approach. Society of Economic Paleontologist and Mineralogist, Special Publications 42, pp. 47–69.
Jordan, T.E., Flemings, P.B., 1991. Large-scale stratigraphic architecture, eustatic variation, and unsteady tectonism: A theoretical evaluation. Journal of Geophysical Research - Solid Earth 96, 6681–6699.
Kaufman, P., Grotzinger, J.P., McCormick, D.S., 1991. Depth-dependent diffusion algorithm for simulation of sedimentation in shallow marine depositional systems. Kansas Geological Survey Bulletin 233, 489–508.
Kim, W., Paola, C., Martin, J., Perlmutter, M., Tapaha, F., 2009. Net pumping of sediment into deep water due to base-level cycling: experimental and theoretical results. In: Kneller, B., Martinson, O.,

McCaffrey, B. (Eds.), External Controls on Deepwater Depositional Systems. SEPM, Special Publication 92, pp. 41–56.
Kominz, M.A., Browning, J.V., Miller, K.G., Sugarman, P.J., Mizintseva, S., Scotese, C.R., 2008. Late Cretaceous to Miocene sea-level estimates from the New Jersey and Delaware coastal plain coreholes: An error analysis. Basin Research 20, 211–226.
Li, Q., Yu, L., Straub, K.M., 2016. Storage thresholds for relative sea-level signals in the stratigraphic record. Geology 44, 179–182.
Liu, X., Rendle-Bühring, R., Henrich, R., 2016. Climate and sea-level controls on turbidity current activity on the Tanzanian upper slope during the last deglaciation and the Holocene. Quaternary Science Reviews 133, 15–27.
Madof, A.S., Harris, A.D., Connell, S.D., 2016. Nearshore along-strike variability: Is the concept of the systems tract unhinged? Geology 44, 315–318.

Miller, K.G., Kominz, M.A., Browning, J.V., Wright, J.D., Mountain, G.S., Katz, M.E., Sugarman, P.J., Cramer, B.S., Christie-Blick, N., Pekar, S.F., 2005. The Phanerozoic record of global sea-level change. Science 310, 1293–1298.
Miller, K., Mountain, G.S., Wright, J.D., Browning, J.V., 2011. A 180 million year record of sea level and ice volume variations from continental margin deep sea isotopic records. Oceanography 24, 40–53.
Miller, K.G., Browning, J.V., Sugarman, P.J., Monteverde, D.H., Andreasen, D.C., Lombardi, C., Thornburg, J., Fan, Y., Kopp, R.E., 2017. Lower To Mid-Cretaceous Sequence Stratigraphy and Characterization of CO2 Storage Potential In the Mid-Atlantic US Coastal Plain. Journal of Sedimentary Research 87, 609–629.
Milliman, J.D., Farnsworth, K.L., 2011. River Discharge to the Coastal Ocean-a Global Synthesis. Cambridge University Press, Cambridge (384 pp.).
Muto, T., Steel, R.J., 2000. The accommodation concept in sequence stratigraphy: some dimensional problems and possible redefinition. Sedimentary Geology 130, 1–10.
Pantopoulos, G., Vakalas, I., Maravelis, A., Zelilidis, A., 2013. Statistical analysis of turbidite bed thickness patterns from the Alpine fold and thrust belt of western and southeastern Greece. Sedimentary Geology 294, 37–57.
Paola, C., 2000. Quantitative models of sedimentary basin filling. Sedimentology 47, 121–178.
Paola, C., Straub, K., Mohrig, D., Reinhardt, L., 2009. The “unreasonable effectiveness” of stratigraphic and geomorphic experiments. Earth-Science Reviews 97, 1–43.
Picard, M.D., 1971. Classification of fine grained sedimentary rocks. Journal of Sedimentary Petrology 41, 179–195.
Posamentier, H.W., Allen, G.P., 1999. Siliciclastic sequence stratigraphy — concepts and applications. Society of Economic Paleontologist and Mineralogist, Concepts in Sedimentology and Paleontology 7 (210 pp.).
Posamentier, H.W., Kolla, V., 2003. Seismic geomorphology and stratigraphy of depositional elements in deep-water settings. Journal of Sedimentary Research 73, 367–388.
Posamentier, H.W., Jervey, M.T., Vail, P.R., 1988. Eustatic controls on clastic deposition I - conceptual framework. In: Wilgus, C.K., Hastings, B.S., Kendall, C.G.S., Posamentier, H.W., Ross, C.A., Van Wagoner, J.C. (Eds.), Sea-level Changes: An Integrated Approach. Society of Economic Paleontologist and Mineralogist, Special Publications 42, pp. 109–124.
Pratson, L.F., Haxby, W.F., 1996. What is the slope of the U.S. continental slope? Geology 24, 3–6.

Prince, G.D., Burgess, P.M., 2013. Numerical modeling of falling-stage topset aggradation: implications for distinguishing between forced and unforced regressions in the geological record. Journal of Sedimentary Research 83, 767–781.
Prosser, I.P., Rustomji, P., 2000. Sediment transport capacity relations for overland flow.
Progress in Physical Geography 24, 179–193.
Rivenæs, J.C., 1992. Application of a dual-lithology, depth-dependent diffusion equation in stratigraphic simulation. Basin Research 4, 133–146.
Rivenæs, J.C., 1997. Impact of sediment transport efficiency on large-scale sequence architecture: results from stratigraphic computer simulation. Basin Research 9, 91–105.
Schieber, J., Zimmerle, W., 1998. The history and promise of shale research. In: Schieber, J., Zimmerle, W., Sethi, P. (Eds.), Shales and Mudstones (vol. 1): Basin Studies, Sedimentology and Paleontology. Schweizerbart'sche Verlagsbuchhandlung, Stuttgart, pp. 1–. 10
Sømme, T.O., Helland-Hansen, W., Granjeon, D., 2009. Impact of eustatic amplitude variations on shelf morphology, sediment dispersal, and sequence stratigraphic interpretation: icehouse versus greenhouse systems. Geology 37, 587–590.
Sylvester, Z., 2007. Turbidite bed thickness distributions: methods and pitfalls of analysis and modelling. Sedimentology 54, 847–870.
Talling, P.J., 2014. On the triggers, resulting flow types and frequencies of subaqueous sediment density flows in different settings. Marine Geology 352, 155–182.
Toucanne, S., Zaragosi, S., Bourillet, J.F., Dennielou, B., Jorry, S.J., Jouet, G., Cremer, M., 2012. External controls on turbidite sedimentation on the glacially-influenced Armorican margin (Bay of Biscay, western European margin). Marine Geology 303, 137–153.
Tucker, G.E., Slingerland, R.L., 1994. Erosional dynamics, flexural isostasy, and long-lived escarpments: A numerical modeling study. Journal of Geophysical Research - Solid Earth 99, 12229–12243.
Urlaub, M., Talling, P.J., Masson, D.G., 2013. Timing and frequency of large submarine landslides: implications for understanding triggers and future geohazard. Quaternary Science Reviews 72, 63–82.
Vail, P.R., Mitchum, R.M., Thompson, J.R., Thompson, S., 1977. Seismic stratigraphy and global changes of sea level, part 4: global cycles of relative changes of sea level. In: Payton, C.E. (Ed.), AAPG Memoir 26 Seismic Stratigraphy – Applications to Hydrocarbon Exploration, pp. 83–97.
Willgoose, G., Bras, R.L., Rodriguez-Iturbe, I., 1991. Results from a new model of river basin evolution. Earth Surface Processes and Landforms 16, 237–254.
Xie, X., Heller, P.L., 2009. Plate tectonics and basin subsidence history. Geological Society of America Bulletin 121, 55–64.
Zhang, J., Steel, R., Olariu, C., 2017. What conditions are required for deltas to reach the shelf edge during rising sea level? Geology 45, 1107–1110.

List of figures

List of tables

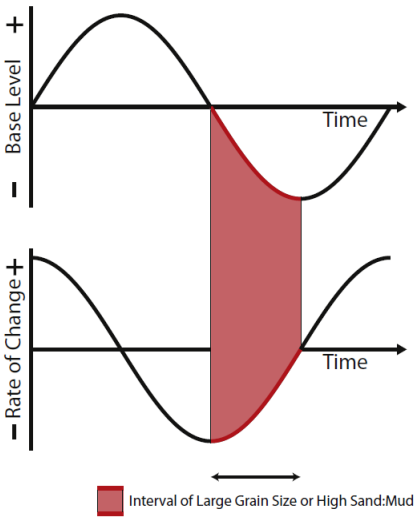

Fig. 1

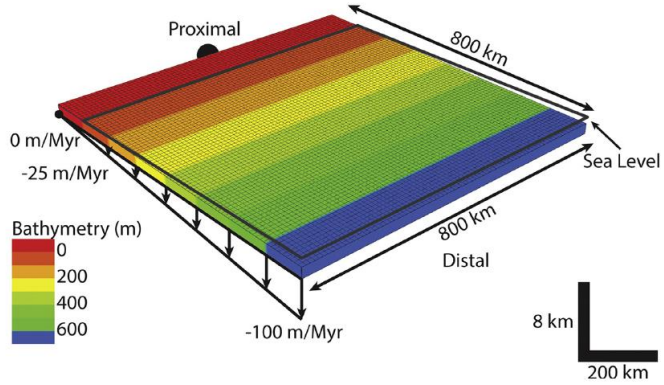

Fig. 2

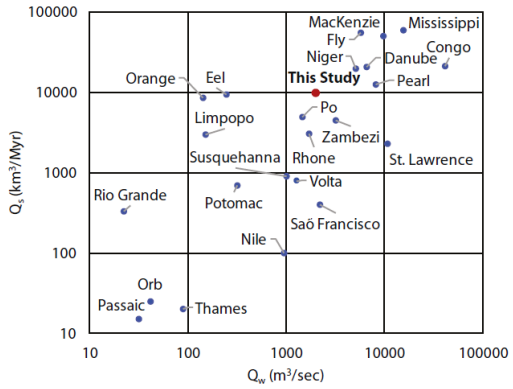

Fig. 3

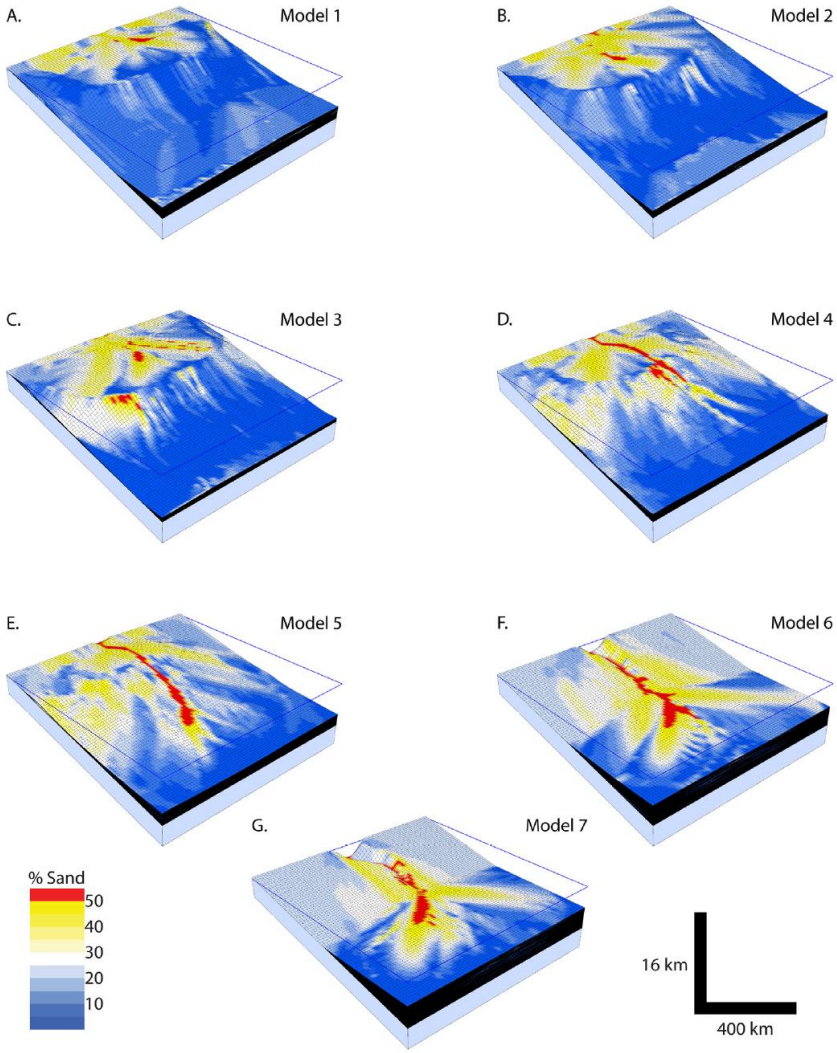
A.
Model 1
B.
Model 2
C.
Model 3
D.
Model 4
E.
Model 5
F.
Model 6
G.
Model 7
% Sand
50
40
30
20
10
16 km
400 km

Fig. 4

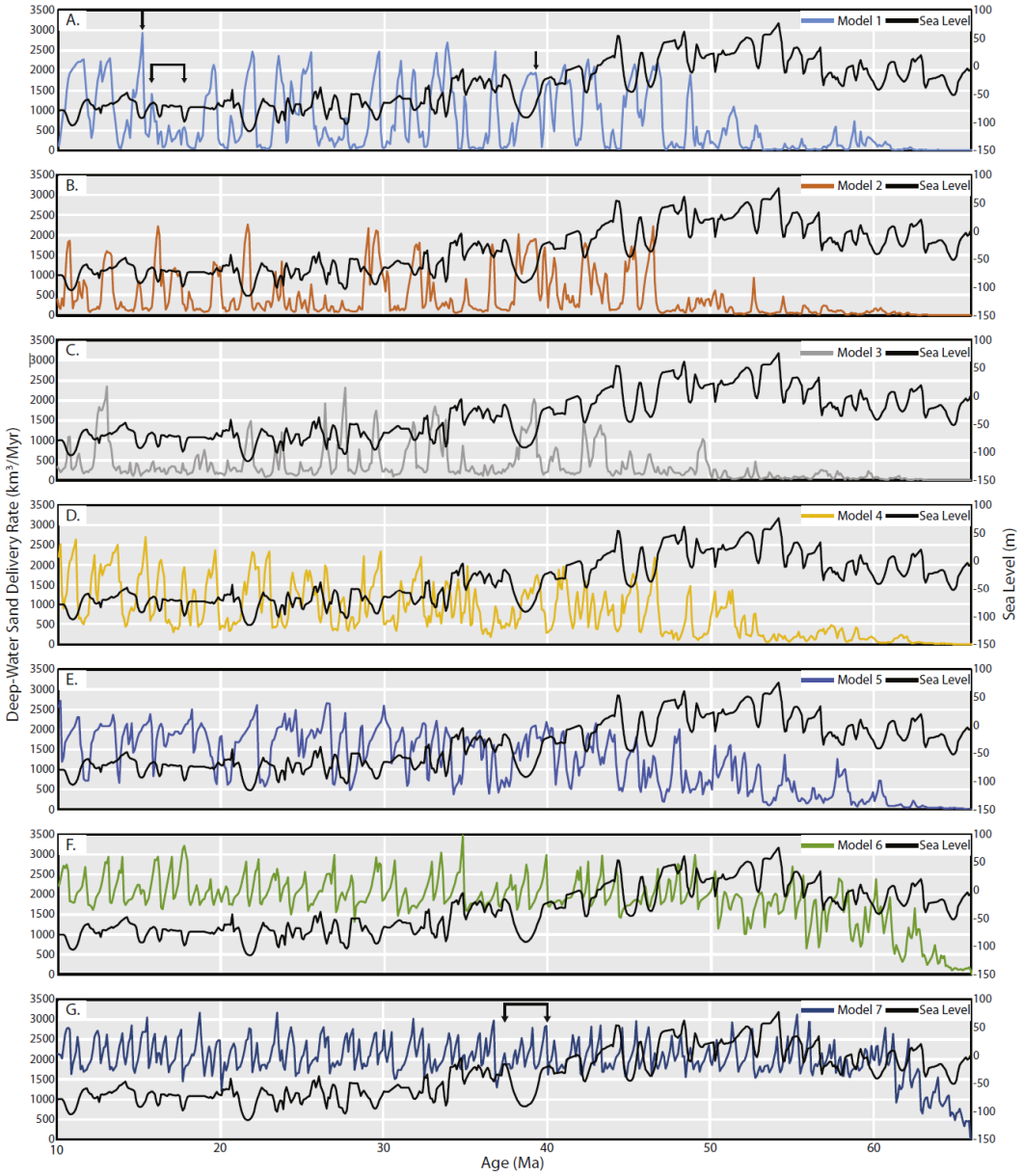
A.
Model 1
Sea Level
B.
Model 2
Sea Level
C.
Model 3
Sea Level
D.
Model 4
Sea Level
E.
Model 5
Sea Level
F.
Model 6
Sea Level
G.
Model 7
Sea Level
Deep-Water Sand Delivery Rate (km³/Myr)
Sea Level (m)
Age (Ma)
0
500
1000
1500
2000
2500
3000
3500
-150
-100
-50
0
50
100
10
20
30
40
50
60

Fig. 5

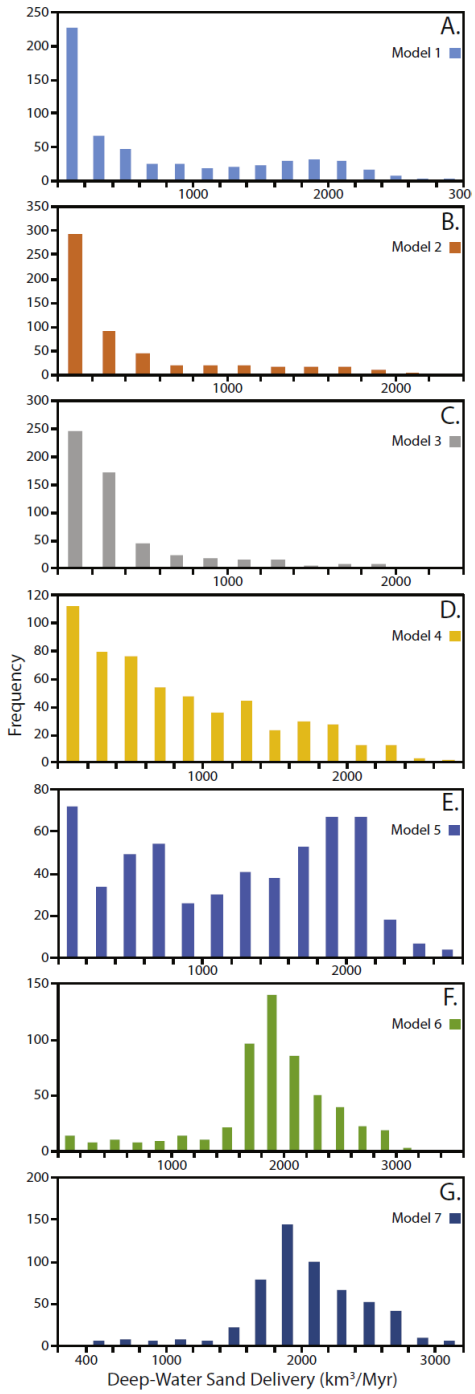
A.
Model 1
B.
Model 2
C.
Model 3
D.
Model 4
E.
Model 5
F.
Model 6
G.
Model 7
Frequency
Deep-Water Sand Delivery (km³/Myr)

Fig. 6

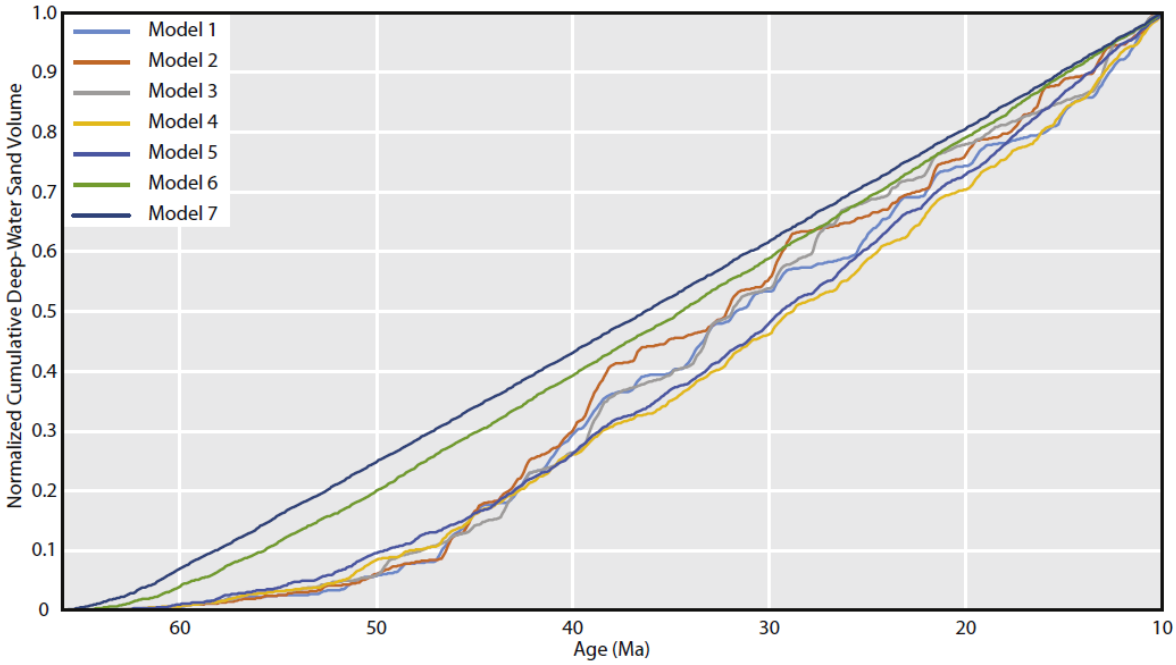
Model 1
Model 2
Model 3
Model 4
Model 5
Model 6
Model 7
Normalized Cumulative Deep-Water Sand Volume
0
0.1
0.2
0.3
0.4
0.5
0.6
0.7
0.8
0.9
1.0
60
50
40
30
20
10
Age (Ma)

Fig. 7

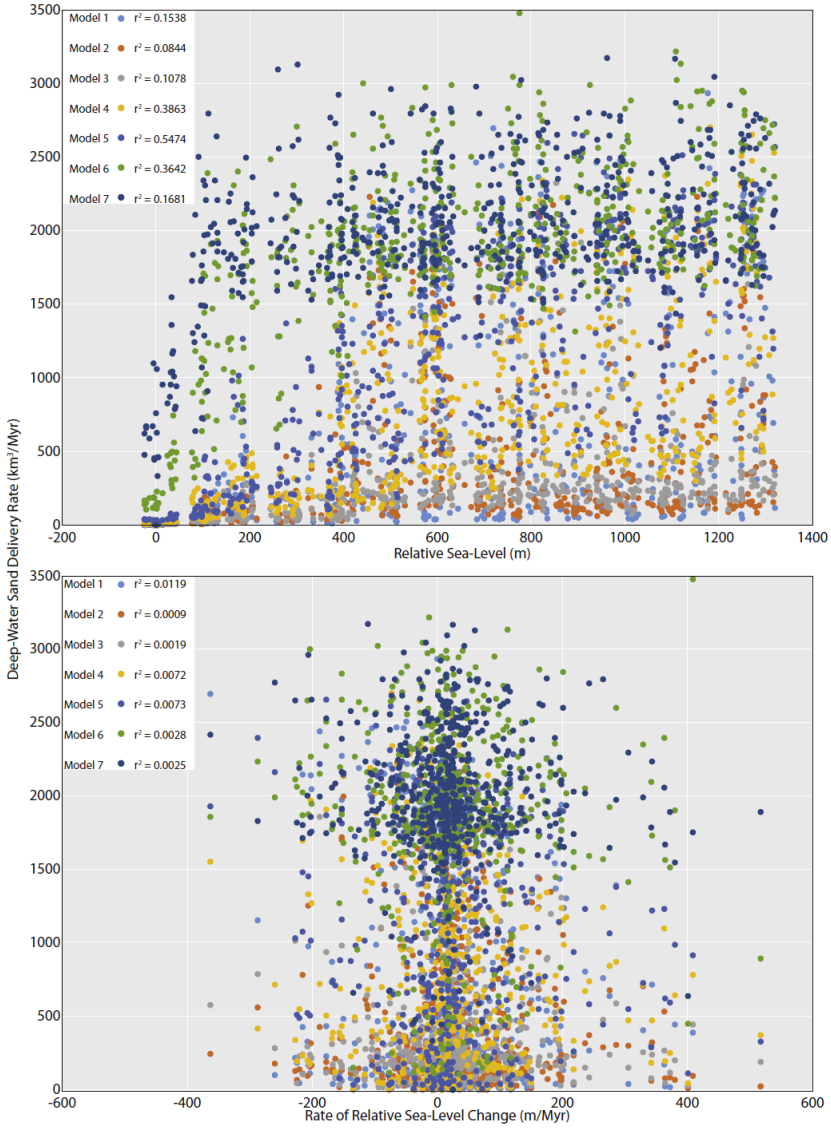
Model 1 r² = 0.1538
Model 2 r² = 0.0844
Model 3 r² = 0.1078
Model 4 r² = 0.3863
Model 5 r² = 0.5474
Model 6 r² = 0.3642
Model 7 r² = 0.1681
Deep-Water Sand Delivery Rate (km³/Myr)
0
500
1000
1500
2000
2500
3000
3500
-200
0
200
400
600
800
1000
1200
1400
Relative Sea-Level (m)
Model 1 r² = 0.0119
Model 2 r² = 0.0009
Model 3 r² = 0.0019
Model 4 r² = 0.0072
Model 5 r² = 0.0073
Model 6 r² = 0.0028
Model 7 r² = 0.0025
0
500
1000
1500
2000
2500
3000
3500
-600
-400
-200
0
200
400
600
Rate of Relative Sea-Level Change (m/Myr)

Fig. 8

Table 1

Parameter	Model 1	Model 2	Model 3	Model 4	Model 5	Model 6	Model 7
Water-driven marine diffusion coefficient for mud (km2/kyr)	0.5	2.5	5.0	25	50	250	500
Water-driven marine diffusion coefficient for sand (km2/kyr)	0.1	0.5	1.0	5.0	10	50	100

Table 2

Parameter	Value	Reference
Domain length (x axis) (km)	800	-
Domain length (y axis) (km)	800	-
Grid spacing (km)	10	-
Run Period (Ma)	66-10	-
Time steps (Myr)	0.1	-
Sediment supply (km3/Myr)	10000	Milliman and Farnsworth (2011)
River discharge (m3/s)	2000	Milliman and Farnsworth (2011)
Gradient of shelf (degrees)	0.06	Pratson and Haxby (1996) Harris et al. (2014)
Gravity-driven terrestrial diffusion coefficient for mud (km2/kyr)	0.001	Harris et al. (2016)
Gravity-driven terrestrial diffusion coefficient for sand (km2/kyr)	0.001	Harris et al. (2016)
Gravity-driven marine diffusion coefficient for mud (km2/kyr)	0.001	Harris et al. (2016)
Gravity-driven marine diffusion coefficient for sand (km2/kyr)	0.001	Harris et al. (2016)
Water-driven terrestrial diffusion coefficient for mud (km2/kyr)	1000	Harris et al. (2016)
Water-driven terrestrial diffusion coefficient for sand (km2/kyr)	250	Harris et al. (2016)
m	1.3	Prosser and Rustomji (2000)
n	1.5	Prosser and Rustomji (2000)
Critical angle of repose for slumping (degrees)	2	Booth et al. (1993)
Maximum erosion rate of sediment (m/Myr)	1000	
Subsidence rate at distal end of model (km/Myr)	100	Xie and Heller (2009)
Sea-level Curve (m)	-	Kominz et al. (2008)

Table 3

	Relative Sea Level			Rate of Relative Sea-Level Change		
Model	r	r2	p value	r	r2	p value
1	0.3922	0.1538	4.57E-22	0.1092	0.0119	0.0097
2	0.2905	0.0844	2.28E-12	0.0299	0.0009	0.4804
3	0.3284	0.1078	1.42E-15	0.0440	0.0019	0.2991
4	0.6216	0.3863	2.88E-61	0.0847	0.0072	0.0449
5	0.7398	0.5474	2.75E-98	0.0856	0.0073	0.0429
6	0.6035	0.3642	5.95E-57	0.0528	0.0028	0.2122
7	0.4100	0.1681	3.74E-24	0.0497	0.0025	0.2408